Development and Characterization of Palm Flower Carbon Reinforced DOPO-Urea Diamine Based Cardanol Benzoxazine-Epoxy Hybrid Composites

Vaithilingam Selvaraj,[1] **Thangavel Ravivarman Raghavarshini**,[1] **Muthukaruppan Alagar**[2]
[1]*Nanotech Research Lab, Department of Chemistry, University College of Engineering Villupuram (A Constituent College of Anna University, Chennai), Kakuppam, Villupuram, Tamil Nadu, India*
[2]*Polymer Engineering Laboratory, PSG Institute of Technology and Applied Research, Neelambur, Coimbatore, 641062, India*

In the present work, amine-functionalized palm flower carbon (*f*-PFC)-reinforced 9, 10-dihydro-9-oxa-10-phosphaphenanthrene-urea diamine-based cardanol benzoxazine-epoxy hybrid (DUDCBz-EP) composites have been developed and characterized. Differential scanning calorimeter analysis indicate that the amine-functionalized palm flower carbon-reinforced cardanol-benzoxazine/epoxy (*f*-PFC/DUDCBz-EP) hybrid composites possess the higher values of glass-transition temperature (T_g) than that of hybrid matrix (DUDCBz-EP). Results from TGA infer that the PFC reinforcement significantly improves thermal stability and char yield according to the percentage weight. Morphological studies ascertain the amorphous structure and uniform as well as homogeneous dispersion of PFC reinforcement in the hybrid matrix. Contact angle measurements indicate that both the hybrid matrix and composites developed in the present work possess hydrophobic behavior. Data obtained from corrosion studies infer that the hybrid matrix as well as hybrid composites exhibit significant corrosion-resistant behavior toward the surface of the steel specimen due to inherent characteristics of both benzoxazine and epoxy matrix, in addition to amine-functionalized PFC. The results obtained from different studies, it is suggested that these hybrid matrix possess significantly improved properties and can be exploited for high-performance cost competitive coatings for different industrial applications including protection of steel surfaces from corrosion. POLYM. ENG. SCI., 00:000–000, 2020. © 2020 Society of Plastics Engineers

INTRODUCTION

Thermosetting polymeric resins and their composites are widely used in different industrial and engineering applications. Among them, bio-based benzoxazines based matrices and composites offer a variety of advantages when compared to those of conventional benzoxazine products. The petrochemical-based raw materials used for the manufacture of polymeric products lead to number of environmental problems. Hence, the researches based on bio-based renewable materials are focused around the world by researchers and academicians toward the production of sustainable monomers, polymeric products [1] and reinforcements [2], and so on.

In order to protect the environment and to minimize the pollution, the need of utilization of sustainable bio-based materials is warranted for the production of chemical intermediates, monomers, and polymers, according to 12 principles of green chemistry [3]. The design and development of cyclic molecules may lead to form three-dimensional crosslinked network structured polymeric materials become powerful strategy, because these materials expected to possess unique properties and performances [4]. In this context, the cyclic benzoxazine macromers play an important role, among thermosetting resins, since it undergoes ring-opening polymerization reaction in the absence of any catalyst at different temperatures and also releases no by-products during curing process. Further, it is also possible to make structural modifications by coupling or blending with other polymeric materials like polyimide, cyanate ester, epoxy, and polyurethane resins to improve thermal, mechanical, dielectric, surface, and morphology including toughness of the benzoxazine resins [5, 6].

It is well known that the most of the bio-based polybenzoxazines possesses lower crosslinking density and limited thermomechanical properties. Hence, the enhancements of properties of bio-based benzoxazines are necessitated by coupling or hybridizing with multifunctional monomeric or polymeric intermediates. It was reported that the cardanol-based benzoxazine blended with epoxy resin significantly improved the processability, which also acts as property modifier and crosslinker including makes the hybrid material become cost-effective with high-performance properties [7–9]. In the recent past, with a view to improve thermal stability and flame-retardant behavior of benzoxazines, the 9, 10-dihydro-9-oxa-10-phosphaphenanthrene 10-oxide (DOPO) was incorporated and found that there was a significant enhancement in the values of degradation temperature, glass-transition temperature (T_g), and char yield [10].

Polymeric resins, when reinforced with cashew nut shell carbon [11], crab shell [12], chitosan [13], timber [14], cellulose [15], lignin [16] and sisal fiber, and so on, improve the properties to an appreciable extent and become useful for number of high-performance applications. The natural fillers [17] reinforced polybenzoxazine composites show significant improvement in the physical, corrosion resistant, thermal, and dielectric properties [18]. Polybenzoxazines possess an excellent surface properties, which make them suitable for hydrophobic and corrosion-resistant applications [19, 20]. In the present work, an attempt has been made to hybridize DOPO amine-based cadanol-benzoxazine with epoxy resin in order exploit the benefits of both resins and the hybrid matrix resin resulted was reinforced with varying weight percentages of amine-functionalized palm flower carbon (*f*-PFC) to obtain benzoxazine-epoxy composites. The hybrid matrix and composites obtained were characterized by different analytical

Correspondence to: V. Selvaraj; e-mail: rajselva_77@yahoo.co.in
DOI 10.1002/pen.25331
Published online in Wiley Online Library (wileyonlinelibrary.com).

techniques and the data resulted from different studies are discussed and reported.

EXPERIMENTAL

Materials

9, 10-Dihydro-9-oxa-10-phosphaphenanthrene 10-oxide (DOPO), para formaldehyde, chloroform, sodium hydroxide, tetrahydro furan (THF), and toluene were purchased from Alpharm fine chemicals. Concentrated sulfuric acid (Con.H_2SO_4), ammonium peroxo disulphate, ethanol, triethylenetetramine, and methanol were procured from Merck Millipore. Urea was obtained from Loba Chemie. LY 556 epoxy resin and Aradur140 were procured from Hindustan Ciba Giegy Ltd. Mumbai, India. Cardanol was acquired from Satya Cashew Chemicals Pvt. Ltd. Chennai, India. Palm flower was collected from Pathirakottai, Panruti, Cuddalore districts, Tamil Nadu, India.

Synthesis of DOPO-Urea Diamine

A mixture of 1.06 g of DOPO and 0.05 g of urea was taken in a round bottomed flask and melted at 120–130°C. The resulted melt was stirred at 130°C for 3 h and the progress of the reaction was monitored and confirmed by thin layer chromatography method. After the completion of reaction, the reaction temperature was brought to 100°C and 2.5 mL of toluene was added to the reaction product, which precipitates the resulted DOPO-urea diamine (DUD) compound. The obtained precipitate was filtered and washed with toluene. The resulted solid product was recrystallized with tetra hydro furan (THF) as per the previous report [21, 22]. A glassy substance was obtained and dried to get a white solid of DUD (Fig. 1).

Preparation of f-*PFC*

The PFC was prepared as per the previous report [23]. Palm flower obtained from local area was sun light dried, cut in to small pieces, and heated at 350–400°C in a silica crucible to obtain palm carbon, which was soaked in 1:1 ratio of conc. H_2SO_4:H_2O for 48 h. Then the reaction mixture was filtered, washed with water and the filtered carbon material was kept in an oven at 100°C for 48 h to remove the water and to get dry PFC. Then, the freshly prepared saturated ammonium per sulphate solution was added to 200 mL 2 mol.H_2SO_4 solution. To this reaction mixture, 5 g of PFC was added and the stirring was continued for another 24 h, which was then filtered and washed with water and ethanol [24]. Finally, the obtained carbon was dried at 100°C for 24 h to get oxidized form of the carbon from PFC. A 1 g of triethylenetetramine (TETA) was mixed with 30 mL of methanol under reflux condition for 30 min and then 2.5 g of oxidized PFC was added and stirred for 8 h under reflux condition. Then, the reaction product was filtered, washed with methanol and then dried at 100°C for 24 h to get an *f*-PFC (Sch. 1).

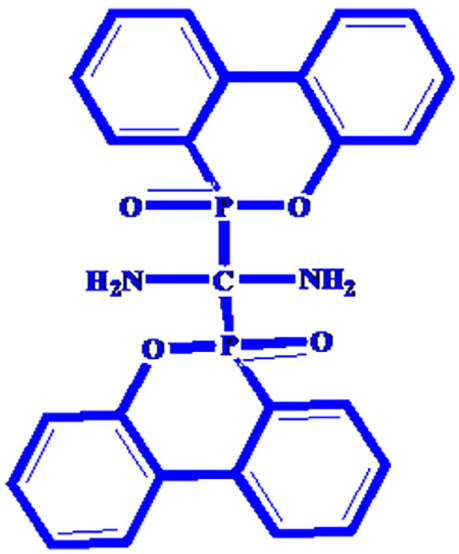

FIG. 1. Structure of the DUD compound. [Color figure can be viewed at wileyonlinelibrary.com]

Preparation of DUD-Based Cardanol-Benzoxazine

About 3.3 g of DUD and 0.7 g of paraformaldehyde were dissolved in 50 mL of methanol and refluxed at 85°C for an hour. To that reaction mixture, 5 g of cardanol was added and the temperature was raised to 120–130°C and maintained for 36 h. Then, the reaction product obtained was poured in to 2 N sodium hydroxide and the product was extracted using chloroform. The product in the organic layer was dried over anhydrous sodium sulphate and the chloroform was removed under reduced pressure [25]. The obtained pinkish red gel DOPO-urea diamine-based cardanol benzoxazine (DUDCBz) monomer was preserved for further use.

Preparation of f-*PFC/DUDCBz-EP Composites*

A 2 g of DUDCBz monomer, 2 g of epoxy resin, and 0.5 g of Aradur-140 were taken in 20 mL of $CHCl_3$ and stirred for 1 h. The homogeneous solution obtained was poured into silane-coated glass plate and the glass plate was kept in the oven for curing. The temperature was slowly raised and cured at 40, 60, 80 100, 120, 160, 180, 200, 220, 240, and 260°C for each 1 h. The above process was also followed for the preparation of palm flower carbon (*f*-PFC)-reinforced cardanol-benzoxazine-epoxy composites (Sch. 1).

Characterization Techniques

Fourier transform infrared spectra (FTIR) have been carried out by using Perkin Elmer spectrometer with KBr disk for *f*-PFC sample while without KBr for neat DUDCBz-EP matrix and 1, 3, and 5 wt% of *f*-PFC incorporated DUDCBz-EP composite films. The morphological images were obtained using scanning electron microscope (SEM) of JEOL JSM-5610LV. X-ray diffraction (XRD) analysis was carried out in the ambient temperature using a Rich Seifert (Model 3000) with the diffraction angle at 2θ from 0 to 90. Thermogravimetric analysis (TGA) was carried out using METTLER TOLEDO micro and ultra-micro balances with submicrogram resolution at a temperature range up to 800°C. Differential scanning calorimeter (DSC) curves were obtained using DSC Q200 V23.10 Build 79 model over a temperature range of 0–300°C. The hydrophobic nature of the composites was studied using contact angle instrument Model OCA EC15 from Data Physics, GmbH (Germany). Corrosion studies were carried out using biologic VSP2 multichannel (France) workstation analyzer and the data obtained are interpreted with help of Tafel plot.

DOI 10.1002/pen

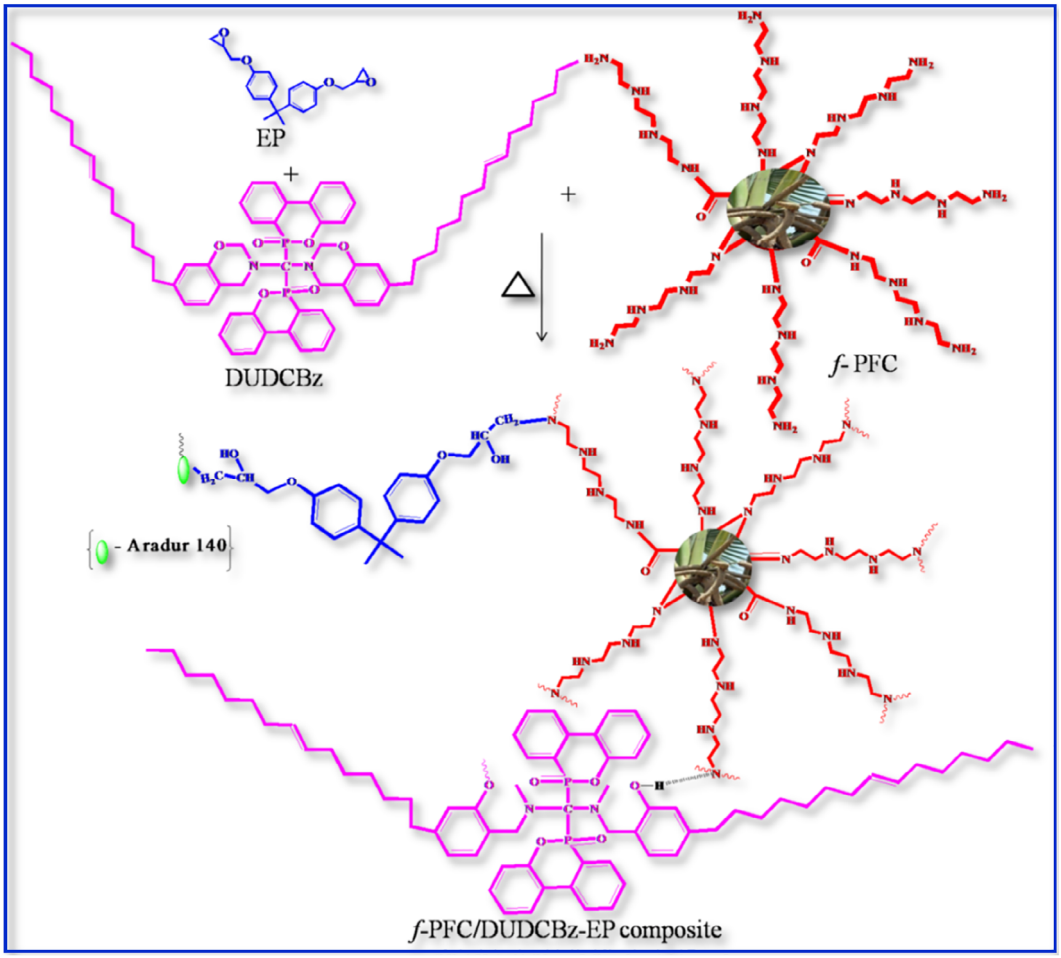

Sch 1. Preparation of *f*-PFC-reinforced DOPO-urea diamine-based cardanol-benzoxazine-epoxy composites (*f*-PFC/DUDCBz-EP). [Color figure can be viewed at wileyonlinelibrary.com]

RESULTS AND DISCUSSION

FTIR Studies

Figure 2 shows the FTIR spectra of *f*-PFC, DUD, DUDCBz monomer, DUDCBz matrix, DUDCBz-EP blended matrix, and varying weight percentages of *f*-PFC-reinforced DOPO-urea diamine based cardanol benzoxazine-epoxy (*f*-PFC/DUDCBz-EP) composites. From the FTIR spectrum of *f*-PFC compound, the peak noticed at 3,334 cm^{-1} indicates the presence of N—H stretching vibration of triethylene tetramine (TETA). The peak observed at 1596 cm^{-1} in *f*-PFC spectrum was attributed due to the presence of carbonyl (C═O) group. In addition to N—H stretching, the peaks obtained at 2,956 cm^{-1} and 2,865 cm^{-1} in *f*-PFC spectrum are attributed to aliphatic —CH_2 group of TETA compound [26]. Therefore, the resulted characteristic IR spectra patterns confirm the *f*-PFC.

From the FTIR spectrum of DOPO-urea based diamine (DUD), the absorption peaks obtained at 1,252 cm^{-1} and 972 cm^{-1} are corresponding to —P—O—Ph and P—O—C stretching vibration obtained from DOPO compound. The peak appeared at 1,450 cm^{-1} in DUD compound represents the C—N stretching vibrations obtained by the reaction with urea compound. The vibration absorption peak occurred at 3,342 cm^{-1} in DUD compound was assigned to N—H stretching of the urea molecule [27]. In DOPO compound, the peak obtained at 2,403 cm^{-1} denotes

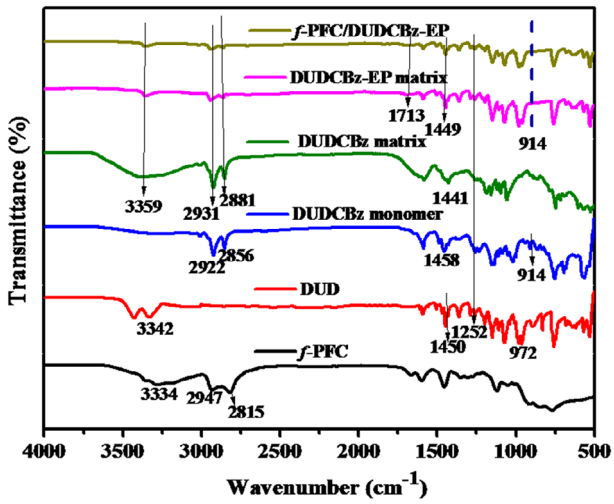

FIG. 2. FTIR spectra of *f*-PFC, DUD, DUDCBz monomer, cured DUDCBz matrix, DUDCBz-EP matrix and varying weight percentages of *f*-PFC-reinforced DOPO-urea diamine-based cardanol benzoxazine-epoxy polymer composites. [Color figure can be viewed at wileyonlinelibrary.com]

(P—H) the active hydrogen, which was absent in DUD compound [28, 29] and this result concludes that the active hydrogen from DOPO compound reacted with carbonyl group of urea to form a

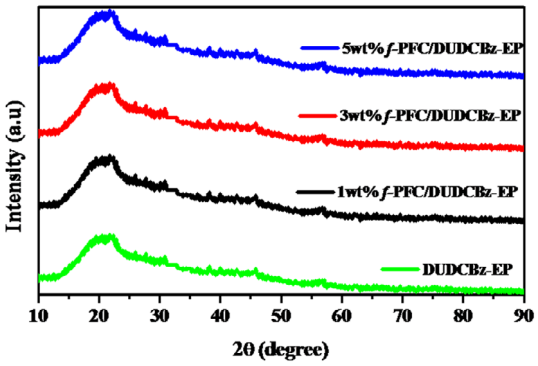

FIG. 3. XRD spectra of DOPO urea diamine-based cardanol benzoxazine-epoxy matrix and palm flower carbon-reinforced composites. [Color figure can be viewed at wileyonlinelibrary.com]

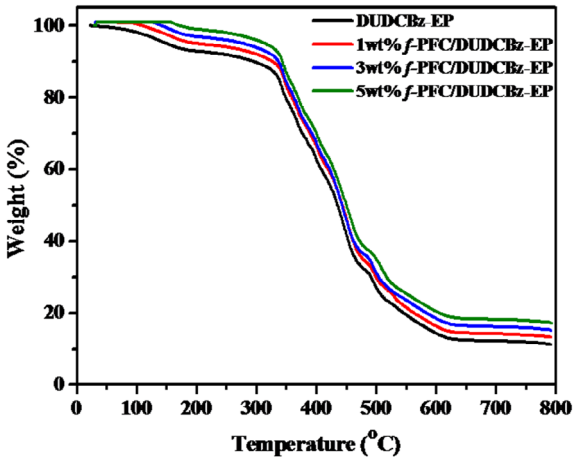

FIG. 5. TGA curves of DOPO urea diamine-based cardanol-benzoxazine-epoxy matrix and *f*-PFC/DUDCBz-EP hybrid composites. [Color figure can be viewed at wileyonlinelibrary.com]

new DOPO-urea-based diamine (DUD). Further, the appearance of new band around 914 cm^{-1} in DUDCBz monomer confirms the benzoxazine ring formation from DUD, cardanol, and paraformaldehyde. The vibration peaks appeared at 1,458 cm^{-1} and 2,922 cm^{-1} and 2,856 cm^{-1} are assigned to C—N stretching and CH_2 stretching vibrations, respectively [30]. From IR spectra, it concluded the formation of DUDCBz monomer.

FTIR spectrum of DUDCBz polymer matrix has the absorption peak obtained at 3,352 cm^{-1}, which indicates the existence of inter-molecular hydrogen bonding of —O···H···N [31]. The absorption peaks visible at 2,925 cm^{-1} and 2,859 cm^{-1} represent the aliphatic —CH_2 group of the cardanol molecules. The peak disappeared at 914 cm^{-1} in DUDCBz matrix infers the cleavage of benzoxazine ring structure and this result ascertain the occurrence of polymerization during the formation of DUDCBz matrix through thermal curing process [32].

Further, the FTIR spectra of DOPO-urea diamine-based cardanol benzoxazine-epoxy (DUDCBz-EP) matrix and amine functionalized palm flower carbon reinforced DOPO-urea diamine based cardanol benzoxazine-epoxy (*f*-PFC/DUDCBz-EP) composite films confirm the disappearance of characteristic absorption band at 914 cm^{-1} that was corresponding to benzoxazine ring. This is results further ascertain the formation of DUDCBz-EP matrix and *f*-PFC/DUDCBz-EP composites through the Mannich reaction [33]. The absorption peak appeared at 1,449 cm^{-1} is attributed to the C—N bond and the C═O vibration peak has been visualized at 1,713 cm^{-1}. The peak obtained at 3,359 cm^{-1} is also corresponding to the hydrogen bonding of N····H····O [34–36],

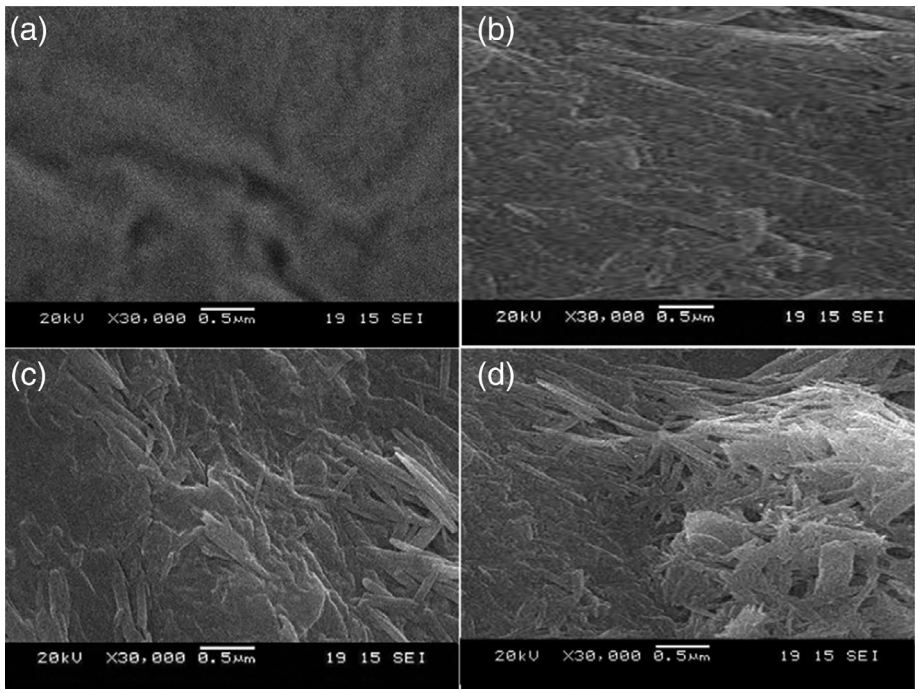

FIG. 4. SEM images of (a) DUDCBz-EP, (b) 1 wt% *f*-PFC/DUDCBz-EP, (c) 3 wt% *f*-PFC/DUDCBz-EP, and (d) 5 wt % *f*-PFC/DUDCBz-EP hybrid composites.

DOI 10.1002/pen

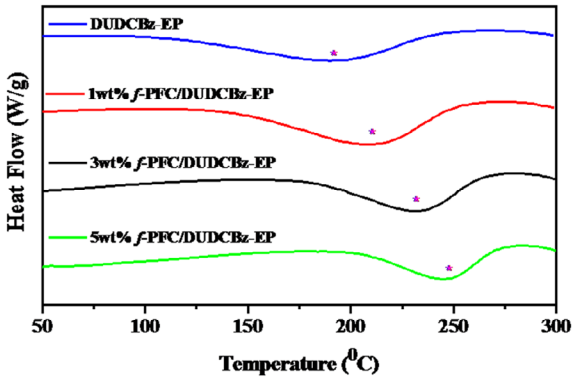

FIG. 6. DSC thermograms of DUDCBz-EP and different weight percentages of *f*-PFC/DUDCBz-EP hybrid composites. [Color figure can be viewed at wileyonlinelibrary.com]

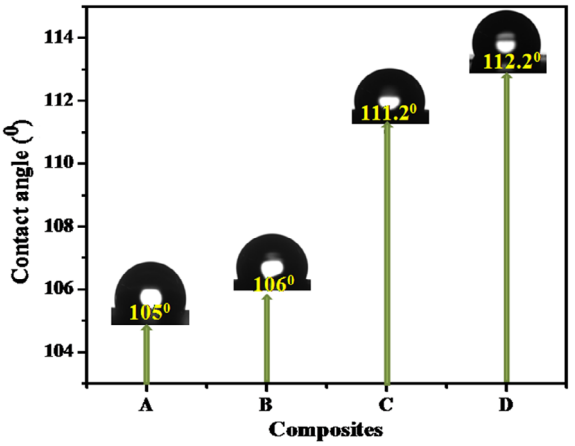

FIG. 7. Contact angle values of (a) DUDCBz-EP, (b) 1 wt% *f*-PFC/DUDCBz-EP, (c) 3 wt% *f*-PFC/DUDCBz-EP, and (d) 5 wt% *f*-PFC/DUDCBz-EP hybrid composites. [Color figure can be viewed at wileyonlinelibrary.com]

which may be resulted due to the cross linking polymerization that was occurred during thermal curing process of DUDCBz-EP with *f*-PFC reinforcement. Hence, FTIR spectra studies infer that the *f*-PFC was chemically bonded with DUDCBz-epoxy matrix to produce crosslinked *f*-PFC/DUDCBz-EP composites.

XRD Studies

Further to investigate the structure of cardanol-benzoxazine-epoxy matrix and *f*-PFC incorporated cardanol benzoxazine-epoxy composites, a wide angle XRD pattern for DUDCBz-EP, 1 wt% *f*-PFC/DUDCBz-EP, 3 wt% *f*-PFC/DUDCBz-EP, and 5 wt% *f*-PFC/DUDCBz-EP hybrid composites were studied (Fig. 3). From Fig. 3, it was observed that all the hybrid composites and matrix have been shown a broad peak with the maximum peak intensity at around $2\theta = 20°$ indicating the amorphous nature of the hybrid DUDCBz-EP matrix [37]. In addition, XRD patterns also indicate that the *f*-PFC/DUDCBz-EP hybrid composite films possess an amorphous morphology even after the addition of the reinforcement of *f*-PFC and confirming the complete intercalation of *f*-PFC phase in DUDCBz-EP matrix [38].

SEM Images

The surface morphology of DUDCBz-EP hybrid matrix and *f*-PFC/DUDCBz-EP hybrid composites was studied by SEM (Fig. 4). The dispersion of PFC in DUDCBz-epoxy hybrid matrix was observed as fiber-like structure, which supports the enhanced properties of the hybrid composites [39]. However, the DUDCBz-EP hybrid matrix shows a smooth fractured surface and fiber-like structures were developed in the composite materials. The smooth surface along with exfoliated structure present in the DUDCBz-epoxy composites were noticed without any agglomeration even at 5 wt% *f*-PFC/DUDCBz-EP composites. This result confirms the homogenous and molecular level dispersion of PFC due to enhanced compatibility and efficient chemical interaction exists between the reinforcement and DUDCBz-EP matrix. In addition, the fiber-like structure formation was also observed from the cross-sectional view of the composites indicating improved properties of the composites [40].

Thermal Studies

TGA were also carried out for DUDCBz-EP hybrid matrix and PFC-reinforced DUDCBz-EP hybrid composites (Fig. 5). The 5% weight loss took place at 289°C for DUDCBz-EP matrix and for 5 wt% *f*-PFC/DUDCBz-EP composites at 322°C, which may explained due to the improved complexity and the formation of network structure brought by the reinforcement [41]. The char yield of 5 wt% *f*-PFC/DUDCBz-EP composites is about 18%, whereas that of DUDCBz-EP hybrid matrix was 11% and the

TABLE 2. The average contact angle values measured for DUDCBz-EP matrix and (1, 3, and 5 wt%) *f*-PFC/DUDCBz-EP composites at three different points in the same sample.

Samples	Average contact angle with average mean std. deviation (°)
DUDCBz-EP	105.0 ± 0.13
1 wt% *f*-PFC/DUDCBz-EP	106.0 ± 0.18
3 wt% *f*-PFC/DUDCBz-EP	111.2 ± 0.20
5 wt% *f*-PFC/DUDCBz-EP	112.2 ± 0.11

TABLE 1. Thermal properties of DUDCBz-EP hybrid matrix and *f*-PFC/DUDCBz-EP hybrid composites.

S.no	Samples	T_g (°C)	Wt. loss (5%) (°C)	Wt. loss (10%) (°C)	T_{max} (°C)	Char yield (%) at 800 (°C)
1	DUDCBz-EP	197.2	289.3	328.2	517.1	11.39
2	1 wt% *f*-PFC/DUDCBz-EP	207.5	294.9	342.7	527.5	14.19
3	3 wt% *f*-PFC/DUDCBz-EP	231.3	302.1	346.5	537.0	16.18
4	5 wt% *f*-PFC/DUDCBz-EP	245.8	322.3	397.7	548.8	17.58

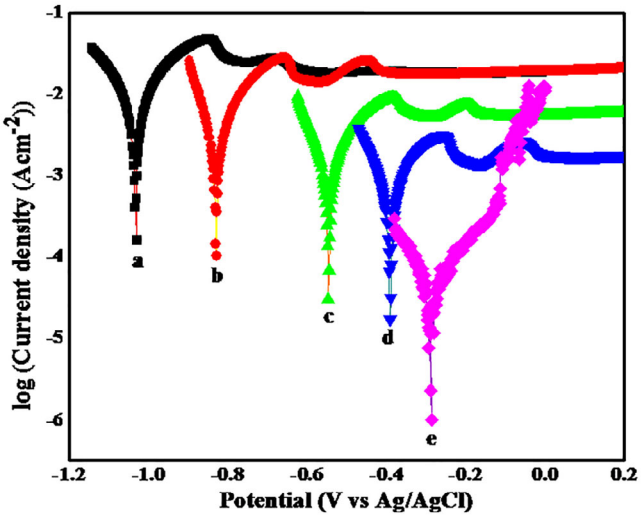

FIG. 8. Tafel plots (a) mild steel, (b) DUDCBz-EP/MS, (c) 1 wt% *f*-PFC/DUDCBz-EP/MS, (d) 3 wt% *f*-PFC/DUDCBz-EP/MS, and (e) 5 wt% *f*-PFC/DUDCBz-EP hybrid composites. [Color figure can be viewed at wileyonlinelibrary.com]

enhanced char yield values of hybrid composites confirm the improved thermal stability [42].

The glass-transition behavior of DUDCBz-EP matrix and *f*-PFC/DUDCBz-EP composites are investigated by DSC studies (Fig. 6). DUDCBz-EP matrix exhibits a T_g of 197°C (Table 1). The T_g value is increased to 246°C for 5 wt% *f*-PFC/DUDCBz-EP composites when compared to that of DUDCBz-EP matrix (197°C), which is due to fiber-like structure formation demonstrating the reinforcing effect of *f*-PFC on *f*-PFC/DUDCBz-EP composites [43] and restrict the mobility of molecular segments in the composite systems.

TABLE 3. T-test values for various weight percentages of (1, 3, and 5 wt%) *f*-PFC/DUDCBz-EP composites with respect to DUDCBz-EP matrix.

S.no.	Samples compared	T-value	*P*-value	Remarks
1.	DUDCBz-EP matrix versus 1 wt% *f*-PFC/DUDCBz-EP composites	−5.5678	0.00255	(0.05) significant
2.	DUDCBz-EP matrix versus 3 wt% *f*-PFC/DUDCBz-EP composites	−32.3784	<0.00001	(0.05) significant
3.	DUDCBz-EP matrix versus 5 wt% *f*-PFC/DUDCBz-EP composites	−49.7832	<0.00001	(0.05) significant

Hydrophobic Studies

The contact angle studies were carried out for DUDCBz-EP hybrid matrix and *f*-PFC/DUDCBz-EP hybrid composites in order to confirm their hydrophobic character. In Fig. 7, 5 wt% *f*-PFC/DUDCBz-EP composite shows the higher value of contact angle of 112.2°, which confirms the improved hydrophobic behavior of the polymeric composite films. The contact angles were measured at three different places on the same sample and their average values are reported for DUDCBz-EP matrix and *f*-PFC (1, 3, and 5 wt%)/DUDCBz-EP composites. The average contact angle values with their uncertainty for the obtained three values [44–47] are given in Table 2. In addition, the contact angle results conclude that both the hybrid matrix and composite materials are hydrophobic in nature [45].

Further, the contact angle values of DUDCBz-EP matrix and *f*-PFC/DUDCBz-EP composites were statistically analyzed by applying *t*-test in accordance with the previous reports [48–51]. *T*-Test was calculated by computation method and results of the *t*-test were compared between the DUDCBz-EP matrix and various weight percentages of (1, 3, and 5 wt%) *f*-PFC/DUDCBz-EP composites (Table 2). From the t-Test results (Table 3), it was concluded that there was a significant difference observed between DUDCBz-EP matrix and 1, 3, and 5 wt% *f*-PFC/DUDCBz-EP composites. Further, the observed *P* values (Table 3) are less than 0.05 and these results confirm the significant effect of water repellent behavior for DUDCBz-EP matrix with the incorporation of varying weight percentages of *f*-PFC content that results *f*-PFC/DUDCBz-EP composites.

Anticorrosion Properties

Electrochemical measurements were carried out by using biologic VSP2 multichannel (France) workstation analyzer with two electrode system, in which the coated sample was used as the working electrode and Ag/AgCl (saturated KCl) electrode as the reference electrode [52]. The area of working electrode is 1×1 cm^2. All tests were performed in a corrosive medium of synthetic sea water (3.5 wt% NaCl) at an ambient temperature and the process was repeated at least for three times to ensure accuracy (Figure 8).

The corrosion potential (E_{corr}) and corrosion current (I_{corr}) were obtained from the Tafel plots (Table 4). From Tafel graph, the corrosion rate can be obtained from *Eq. 1*,

TABLE 4. Electrochemical parameters for MS and MS plates coated with various substrates.

Samples	I_{corr} (Acm^2)	E_{corr} (V)	Corrosion rate (mm/year)	ŋ (%)
Mild steel	−2.0604	−1.1159	148.15	—
DUDCBz-EP/MS	−2.4623	−0.8252	99.08	95.8
1 wt% *f*-PFC/DUDCBz-EP/MS	−2.9376	−0.5488	61.51	97.4
3 wt% *f*-PFC/DUDCBz-EP/MS	−3.2971	−0.3917	42.91	98.2
5 wt% *f*-PFC/DUDCBz-EP/MS	−4.3071	−0.2861	15.58	99.3

DOI 10.1002/pen

$$\text{Corrosion rate} = \frac{K \times EW \times I_{corr}}{\rho A}. \quad (1)$$

where K is a corrosion rate constant with a value 3,272 mm/year, EW is an equivalent weight of mild steel plate that has a value of 27.9 g, ρ is a density of the mild steel plate with a value of 7.85 g cm^{-3}, and A is the sample area (1 × 1 cm^2)

From the results (Table 4), it was noticed that the rate of corrosion was decreased from 148.15 mm/year to 15.58 mm/year with the introduction of *f*-PFC reinforcement in the DUDCBz-EP hybrid matrix coated on mild steel plate. The corrosion protection efficiency (ŋ) has been calculated from *Eq*. 2 utilizing the corrosion current (I_{corr}) as given in Table 4.

$$\eta\,(\%) = \frac{I^0corr - Icorr}{I^0corr} \times 100 \quad (2)$$

where I^0_{corr} is the current density of the mild steel and I_{corr} is the current density of prepared substrate-coated mild steel plates.

From Table 4, it was observed that the I_{corr} decreases from mild steel to 5 wt% *f*-PFC/DUDCBz-EP hybrid composites coated mild steel. Hence, it is inferred that the corrosion protection behavior of both the hybrid matrix and composites is significantly high. However, the corrosion protection efficiency of 5 wt% *f*-PFC/DUDCBz-EP hybrid composites coated mild steel is 99.3%, which is higher than that of DUDCBz-EP hybrid matrix-coated mild steel (95.8%). The increasing performance of corrosion resistance may be explained due to the improved and efficient adhesion results between epoxy-based hybrid samples and steel as well as water-resistant surface behavior offered by cardanol-based benzoxazine moiety coupled with functionalized PFC reinforcement. From the results obtained, it was concluded that the hybrid composites developed in the present work can be considered as surface protection material for steel surface under corrosive environment [53].

The corrosion usually takes place through the redox reaction of iron and oxygen in the presence of water or moisture in the air. Rust may consists of any one of these form or combined form of hydrated iron (III) oxides ($Fe_2O_3{\cdot}nH_2O$), iron(III) oxide-hydroxide (FeO(OH), and $Fe(OH)_3$. The occurrence of process of corrosion involved in the steel may be explained according to *Eqs*. *3–8*.

$$Fe \rightarrow Fe^{2+} + 2e^- \quad (3)$$

$$Fe^{2+} \rightarrow Fe^{3+} + e^- \quad (4)$$

$$O_2 + 2H_2O \rightarrow 4OH^- \quad (5)$$

$$Fe^{3+} + 3OH^- \rightarrow Fe(OH)_3 \quad (6)$$

$$2Fe^{2+} + 4OH^- \rightarrow 2Fe(OH)_2 \rightarrow Fe_2O_3.H_2O \quad (7)$$

$$2Fe^{2+} + O_2 + 2H_2O \rightarrow 2FeOOH + 2H^+ \quad (8)$$

The corrosion mechanism authenticates that the H_2O/moisture and oxygen are the essential components that can cause corrosion and rust formation process in iron- and steel-based products. The incursion of oxygen and water or moisture in the air may be restricted with increasing weight percentage concentrations of amine-functionalized palm flower carbon in polybenzoxazine-epoxy composites, which is in good agreement with the previous report [54]. From corrosion studies, it was ascertained that the hybrid composites developed in the present work can be considered as effective coating material for high-performance corrosion-resistant applications.

CONCLUSIONS

The bio-based DUDCBz-EP hybrid matrix and *f*-PFC/DUDCBz-EP hybrid composites were prepared and their molecular structure, thermal stability, morphology, contact angle, and corrosion-resistant properties were studied by different analytical techniques and methods. From the results, it was concluded that the properties of the benzoxazine were significantly influenced by the presence of *f*-PFC and EP components in the composites. The thermal studies infer that the hybrid composites possess high T_g, thermal stability, and char yield. The XRD and SEM results indicate that *f*-PFC/DUDCBz-EP hybrid composites possess uniform and homogeneous morphology. The value of contact angle studies indicate that the hybrid composites are hydrophobic in nature and the results from corrosion studies ascertain that the *f*-PFC/DUDCBz-EP hybrid composites show the corrosion protection efficiency of 99.3% toward steel surface. Data obtained from different studies, it is suggested that the *f*-PFC/DUDCBz-EP hybrid composites can be efficiently used as a coating materials for high-performance applications.

REFERENCES AND CITED WORK

1. C.F. Wang, C.H. Zhao, J.Q. Sun, S.Q. Huang, X.D. Liu, and T. Endo, *J. Polym. Sci. A Polym. Chem.*, **51**, 2016 (2013).
2. L. Di Landro and G. Janszen, *Compos. Part B*, **67**, 220 (2014).
3. A. Llevot, *J. Am. Oil Chem. Soc.*, **94**, 169 (2016).
4. T. Endo and A. Sudo, *J. Polym. Sci. Part A: Polym. Chem.*, **47**, 4847 (2009).
5. P. Sharma, S. Shukla, B. Lochab, D. Kumar, and P. Kumar Roy, *Mater. Lett.*, **133**, 266 (2014).
6. X.-y. He, J. Wang, N. Ramdani, W.-b. Liu, L.-j. Liu, and L. Yang, *Thermochim. Acta*, **564**, 51 (2013).
7. S. Sahila and L.S. Jayakumari, *Polym. Compos.*, **36**, 1 (2014).
8. S. Rimdusit, P. Kunopast, and I. Dueramae, *Polym. Eng. Sci.*, **51**, 1797 (2011).
9. A. Sudo, R. Kudoh, H. Nakayama, K. Arima, and T. Endo, *Macromolecules*, **41**, 9030 (2008).
10. C. Jubsilp, T. Takeichi, and S. Rimdusit, *Polym. Degrad. Stabil.*, **96**, 1047 (2011).
11. G. Alagumuthu and M. Rajan, *Chem. Eng. J.*, **158**, 451 (2010).
12. H.-J. Liu, X.-M. Wang, W.-J. Cui, Y.-Q. Dou, D.-Y. Zhao, and Y.-Y. Xi, *J. Mater. Chem.*, **20**, 4223 (2010).
13. S.-F. Wang, L. Shen, W.-D. Zhang, and Y.-J. Tong, *Biomacromolecules*, **6**, 3067 (2005).
14. P.l.R. Garcia, C.E. Alfonso, and M. Nieves Gonzalez Garci, *Compos. Part B*, **55**, 528 (2013).
15. J.R. Nair, C. Gerbaldi, A. Chiappone, E. Zeno, R. Bongiovanni, S. Bodoardo, and N. Penazzi, *Electrochem. Commun.*, **11**, 1796 (2009).
16. W. Qin and J.F. Kadla, *Ind. Eng. Chem. Res.*, **50**, 12548 (2011).
17. M.J. John and R.D. Anandjiwala, *Polym. Compos*, **29**, 187 (2008).

18. W.B. Liu, N. Ramdani, and J. Wang, *Advanced and Emerging Polybenzoxazine Science and Technology*, Elsevier, Netherlands, United Kingdom, USA, 499 (2017).
19. H. Zhou, Y. Zhao, H. Wang, and T. Lin, *Adv. Mater. Interfaces*, **3**, 1600402 (2016).
20. X. Feng and L. Jiang, *Adv. Mater.*, **18**, 3063 (2006).
21. W. Chuan Shaq, Y.L. Liu, and Y.S. Chiu, *Polymer*, **43**, 1773 (2002).
22. K. Shree Meenakshi, E. Pradeep Jaya Sudhan, S. Ananda Kumar, and M.J. Umapathy, *Prog. Org. Coat.*, **72**, 402 (2011).
23. M. Srinivas Kini, M.B. Saidutta, and V. Ramachandra Murty, *Int. J. Appl. Eng. Res.*, **10**, 41800 (2015).
24. J. Goscianska, N.A. Fathy, and R.M.M. Aboelenin, *J. Colloid Interface Sci.*, **505**, 593 (2017).
25. V. Selvaraj, K.P. Jayanthi, T. Lakshmikandhan, and M. Alagar, *RSC Adv.*, **5**, 48898 (2015).
26. W.M. Silva, H. Ribeiro, L.M. Seara, H.D.R. Calado, A. S. Ferlauto, R.M. Paniago, C.F. Leite, and G.G. Silva, *J. Braz. Chem. Soc.*, **23**, 1078 (2012).
27. Y.L. Liu, *J. Polym. Sci. A Polym. Chem.*, **40**, 359 (2002).
28. W. Chen, Y. Liu, C. Xu, Y. Liu, and Q. Wang, *RSC Adv.*, **7**, 39786 (2017).
29. J. Grdadolnik and Y. Maréchal, *J. Mol. Struct.*, **615**, 177 (2002).
30. G.J. Abarro, J. Podschun, L.J. Diaz, S. Ohashi, B. Saake, R. Lehnen, and H. Ishida, *RSC Adv.*, **6**, 107689 (2016).
31. Y. Cui, Y. Chen, X. Wang, G. Tian, and X. Tang, *Polym. Int.*, **52**, 1246 (2003).
32. S. Xu, J. He, S. Jin, and B. Tan, *J. Colloid Interface Sci.*, **509**, 457 (2018).
33. D.M. Patil, G.A. Phalak, and S.T. Mhaske, *Prog. Org. Coat.*, **105**, 18 (2017).
34. T. Zhang, J. Wang, T. Feng, H. Wang, N. Ramdani, M. Derradji, X. Xu, W. Liu, and T. Tang, *RSC Adv.*, **5**, 33623 (2015).
35. I. Schnell, S.P. Brown, H.Y. Low, H. Ishida, and H.W. Spiess, *J. Am. Chem. Soc.*, **120**, 11784 (1998).
36. H. Ishida and Y.-H. Lee, *J. Polym. Sci. B Polym. Phys.*, **39**, 736 (2001).
37. H. Guo, J. Zheng, J. Gan, L. Liang, W. Kun, and L. Mangeng, *RSC Adv.*, **5**, 88014 (2015).
38. S. Khan, S. Masood, K. Siddiqui, M. Alam, F. Zafara, Q.M. R. Haque, and N. Nishat, *J. Clean. Prod.*, **196**, 1644 (2018).
39. W. Yang, Y.-R. Zhang, A.C.-Y. Yuen, T.B.-Y. Chen, M.-C. Chan, L.-Z. Peng, W.-J. Yang, S.-E. Zhu, B.-H. Yang, K.-H. Hu, G.-H. Yeoh, and H.-D. Lu, *Chem. Eng. J.*, **321**, 257 (2017).
40. K. Kanimozhi, K. Sethuraman, V. Selvaraj, and M. Alagar, *Front. Chem.*, **2**, 1 (2014).
41. H.-X. Ma, J. Jie Li, J.-J. Qiu, Y. Liu, and C.-M. Liu, *ACS Sustain. Chem. Eng.*, **5**, 350 (2016).
42. K. Sethuraman, P. Prabunathan, and M. Alagar, *RSC Adv.*, **4**, 45433 (2014).
43. X. Wang, S. Zhou, W.-W. Guo, P.-L. Wang, W. Xing, L. Song, and H. Yuan, *ACS Sustain. Chem. Eng.*, **5**, 3409 (2017).
44. J. Dai, N. Teng, X. Shen, Y. Liu, L. Cao, J. Zhu, and X. Liu, *Ind. Eng. Chem. Res.*, **57**, 3091 (2018).
45. A. Tüzün, G. Lligadas, J.C. Ronda, M. Galià, and V. Cádiz, *Eur. Polym. J.*, **69**, 341 (2015).
46. W. Zhang, X. Lu, Z. Xin, and C. Zhou, *RSC Adv.*, **6**, 106054 (2016).
47. D.M. Patil, G.A. Phalak, and S.T. Mhaske, *J. Coat. Technol. Res.*, **14**, 517 (2017).
48. S. Sharma, B.K. Padda, and V. Choudhary, *J. Conserv. Dent.*, **15**, 161 (2012).
49. R. Vadori, M. Misra, and A.K. Mohanty, *J. Appl. Polym. Sci.*, **134**, 44516 (2016).
50. J. A. Kent, A. Winston, W. R. Boyle, W. Loos, and J. E. Ayres, *ORO-628, Isotopes–industrial technology (TID-4500, 41st ed.) ebook* (1965), pp. 1–113.
51. E.V. Bachtiar, K. Kurkowiak, L. Yan, B. Kasal, and T. Kolb, *Polymers*, **11**, 699 (2019).
52. C. Zhou, X. Lu, Z. Xin, and J. Liu, *Corros. Sci.*, **70**, 145 (2013).
53. X. Liu, R. Zhang, T. Li, P. Zhu, and Q. Zhuang, *ACS Sustain. Chem. Eng.*, **5**, 10682 (2017).
54. C.-H. Chang, T.-C. Huang, C.-W. Peng, T.-C. Yeh, H.-I. Lu, W.-I. Hung, C.-J. Weng, T.-I. Yang, and J.-M. Yeh, *Carbon*, **50**, 5044 (2012).